# Synthesis of Fluorinated Graphene/CoAl-Layered Double Hydroxide Composites as Electrode Materials for Supercapacitors

**Article** *in* ACS Applied Materials & Interfaces · January 2017

DOI: 10.1021/acsami.6b11316

CITATIONS
86

READS
245

**3 authors:**

Weijun Peng
Zhengzhou University
**50** PUBLICATIONS **1,176** CITATIONS
SEE PROFILE

Hongqiang Li
Wuhan Institute of Technology
**70** PUBLICATIONS **1,707** CITATIONS
SEE PROFILE

Shaoxian Song
Wuhan University of Technology
**427** PUBLICATIONS **7,813** CITATIONS
SEE PROFILE

ACS APPLIED MATERIALS & INTERFACES

Research Article

www.acsami.org

# Synthesis of Fluorinated Graphene/CoAl-Layered Double Hydroxide Composites as Electrode Materials for Supercapacitors

Weijun Peng, Hongqiang Li, and Shaoxian Song*

Hubei Key Laboratory of Mineral Resources Processing and Environment, School of Resources and Environmental Engineering, and Hubei Provincial Collaborative Innovation Center for High Efficient Utilization of Vanadium Resources, Wuhan University of Technology, Luoshi Road 122, Wuhan, Hubei 430070, China

Supporting Information

**ABSTRACT:** CoAl-layered double hydroxide/fluorinated graphene (CoAl-LDH/FGN) composites were fabricated via a two-step hydrothermal method. The synthesized CoAl-LDH/FGN composites have been characterized by powder X-ray diffraction (XRD), Fourier transform infrared spectroscopy (FT-IR), X-ray photoelectron spectroscopy (XPS), transmission electron microscopy (TEM), field-emission scanning electron microscopy (FESEM), energy dispersive X-ray spectroscopy (EDS), and electrochemical measurements. The results indicated that the fluorinated carbon with various configuration forms were grafted onto the framework of graphene, and the C−F bond configuration and fluorine content could be tuned by the fluorination time. Most of semi-ionic C−F bonds were formed at an appropriate fluorination time and, then, converted into fluorine rich surface groups (such as $CF_2$, $CF_3$, etc.) which were electrochemically inactive as the fluorination time prolonged. Moreover, the CoAl-LDH/FGN composites prepared at the optimal fluorination time exhibited the highest specific capacitance (1222 F/g at 1 A/g), the best rate capability, and the most stable capacitance retention, which offered great promise as electrode materials for supercapacitors.

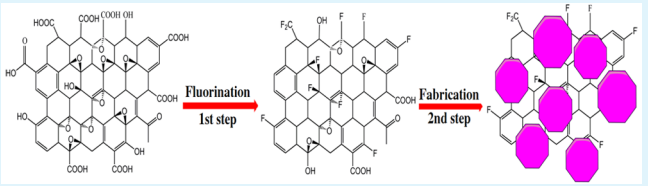


**KEYWORDS:** *CoAl-layered double hydroxide, fluorinated graphene, hydrothermal method, electrochemical performance, supercapacitor*

## 1. INTRODUCTION

The need for renewable energy sources is becoming extremely urgent due to the fast consumption of fossil fuels and tremendous serious environmental issues.[1] Electrochemical materials, considered as a substitution for finite fossil fuels, have attracted more and more concerns because of their high redox reactivity, low-cost, and environmental friendliness.[2,3] The most used electrochemical materials include carbonaceous nanomaterials for electrochemical double layer capacitors and conductive polymers and transition metal (Ni, Ru, Mn, Co, etc.) oxides/hydroxides for pseudocapacitors.[4] Layered double hydroxides (LDHs) containing transition metals (such as Co, Ni, Mn, etc.) are identified as one kind of the most promising electrochemical materials for supercapacitors.[2] LDHs are laminar brucitelike structure with the inserted anion between the positive sandwich.[5] The chemical formula of LDHs is indicated as $[Me^{2+}_{1-x}Me^{3+}_{x}(OH)_2](B^{m-}_{x/m}\cdot nH_2O)$, where $Me^{2+}$ and $Me^{3+}$ stand for bivalent and trivalent cations within the laminar layers, respectively, and $B^{m-}$ stands for an interlaminar anion.[2,6] LDHs have drawn increasing interest due to their unique anisotropy, low cost, high specific capacitance, and ecofriendliness.[7−9] However, the electrochemical performances (ECPs) of LDHs are impeded by their relatively poor electrical conductivity, low power density and mechanical stability, and bad cycle life.[10,11]

To overcome the above hindrances, excellent electroconductive carbon materials, like active carbon,[12] carbon nanoparticles,[12,13] carbon nanotubes,[5,14] carbon nanofibers,[15,16] and graphene (GN),[6,17] have been used to hybridize with LDHs. And the corresponding composites exhibited increased ECPs, like higher specific capacitance and cycling stability and better rate capability.[18] Fluorinated graphene (FGN) is a kind of graphene derivative, in which fluorine atoms are covalently functionalized on carbon nanosheet skeletons.[19,20] FGN is identified as one of the important potential materials due to its increased electrochemical reactivity and outstanding electrode stability,[19] which has been widely used in energy storage devices,[21] catalyst in hydrogen storage,[22] and redox for fuel cell.[23] Feng et al. found that the ECPs of fluorinated graphene hydrogels (FGHs) were better than that of the fluorine-free graphene hydrogel due to the semi-ionic C−F bonds in FGHs facilitated the ion transportation, enhanced the electrical conductivity and provided reactive sites for Faradaic reaction.[24] However, to the best of our knowledge, almost no studies were centered on the hybridization of FGN with LDHs.

In this work, CoAl-LDH/FGN composites were synthesized by a two-step hydrothermal method. The influence of fluorination time on the C−F bond configuration form, fluorine content, and ECPs of the resulting CoAl-LDH/FGN composites were discussed. Compared with pure CoAl-layered

Received: September 7, 2016
Accepted: January 12, 2017
Published: January 18, 2017





DOI: 10.1021/acsami.6b11316
ACS Appl. Mater. Interfaces 2017, 9, 5204−5212

double hydroxide (pLH for short) and CoAl-layered double hydroxide/graphene (abbreviated to LG) composite prepared by the same process, CoAl-LDH/FGN composite exhibited the highest specific capacitance, the best rate capability, and the most stable capacitance retention, making it the most promising electrode material for supercapacitors.

## 2. EXPERIMENTAL SECTION

**2.1. Materials and Chemicals.** Natural flaky graphite with the lateral size of 45 to 38 $\mu$m (exceed 99.9% purity) was used to synthesize GO. $KMnO_4$, $CoCl_3{\cdot}6H_2O$, NaOH, $AlCl_3{\cdot}6H_2O$, $NaNO_3$ and urea in analytical purity, $H_2O_2$ (30%), and HF (40%) were obtained from Sinopharm Chemical Reagent Co., Ltd. (China). Sulfuric acid (98%) and hydrochloric acid (36%) were purchased from Xinyang chemical reagent (China). Deionized water (18.25 MΩ·cm resistivity) was applied in all the work.

**2.2. Preparation and Exfoliation of GN and FGN.** Graphite oxide (GrO) was synthesized according to Hummers method as previously reported.[25−27] FGN was prepared from the as-prepared GrO in the following typical procedures. First, 0.10 g of GrO powder was dispersed in 100 mL of deionized water via a high-shear homogenizer (FLUKO, Germany) with 10000 rpm for 3 min. Next, the GrO suspension was exfoliated via a Sonics ultrasonic processor (750 W, 20 kHz) with 40% amplitude for 10 min. Then, 4 mL of HF was mixed with the GO suspension. After ultrasonic dispersion by a ultrasonic bath (Elmasonic P30H) for 10 min, the mixture was transferred to a 150 mL of Teflon lined autoclave vessel and remained at 150 °C for a regular time interval. Finally, the prepared FGN was washed using deionized water until the supernatant reached neutral by filtration. Furthermore, GN were obtained in the absence of HF with the same process at 150 °C for 12 h. Exfoliation of the as-prepared GN or FGN aggregate was obtained by redispersing it in 25 wt % ethanol solution (1 mg/mL) using the homogenizer and then exfoliated by the ultrasonic processor with 40% amplitude for 15 min. The time intervals for the GO fluorination were 12, 18, and 24 h, and the corresponding FGN suspension were labeled as FGN-12, FGN-18, and FGN-24, respectively.

**2.3. Synthesis of CoAl-LDH/FGN Composites.** A 0.8 mmol portion of $CoCl_3{\cdot}6H_2O$ and 0.4 mmol of $AlCl_3{\cdot}6H_2O$ were dissolved into the above FGN suspension for 2 h stirring. Subsequently, 0.30 g of urea was mixed with the suspension via a stirring for another 0.5 h. The resulting mixture was transferred to the autoclave vessel and remained at 150 °C for 12 h. The synthesized CoAl-LDH/FGN composite was washed with deionized water and ethanol several times by centrifugation prior to drying at 60 °C for 12 h in vacuum. The final composites were labeled as LFG-12, LFG-18, and LFG-24 for the initial feeding of FGN-12, FGN-18, and FGN-24, respectively. For comparison, pLH and LG were fabricated in the absence of FGN and in the presence of GN with the other same experimental condition, respectively. The contents of CoAl-LDH in LG, LFG-12, LFG-18, and LFG-24 were determined by dissolving a weighted amount of the composites with a 1.0 M HCl aqueous solution.[10,28] The content of CoAl-LDH in LG, LFG-12, LFG-18, and LFG-24 were 77.75%, 76.14%, 75.68%, and 75.13%, respectively.

**2.4. Characterizations.** The microstructure and morphology of pLH and LFG-12 were detected using a transmission electron microscope (TEM; JEM2100F, JEOL, Japan) and a field-emission scanning electron microscope (FESEM; S-4800, Hitachi, Japan) with an accelerating voltage of 15 kV, along with energy dispersive X-ray spectroscopy (EDS). Fourier transform infrared (FT-IR) spectra were examined using a Fourier transform infrared spectrometer (Vector-22, Bruker, Germany). X-ray diffraction (XRD) patterns were obtained from a powder X-ray diffractometer (D8 Adwance, Bruker, Germany) equipped with a Cu K$\alpha$ radiation ($\lambda$ = 0.15406 nm) source operated at 40 kV and 100 mA. The specific surface area was achieved by the Brunauer−Emmett−Teller (BET) method, and the measurement was performed according to the physical adsorption of $N_2$ at 77 K via a fully automatic surface area and porosity analyzer (ASAP 2020M, Micromeritics, America). The electrical conductivities of the composites were detected via a four-point configuration (MP-01, Shanghai Advanced Electronic Technology Co., LTD, China) with probe spacing of 2 mm. X-ray photoelectron spectroscopy (XPS; PHI 3056, PERKIN ELMZR, America) with a Mg anode source operated at 15 kV was used to obtain the XPS spectra of the composites.

**2.5. Electrochemical Measurements.** Electrochemical measurements were conducted in a typical three-electrode system on a potentiostat analyzer (VersaSTAT-450, PAR, USA) at room temperature. A saturated calomel electrode, 1.5 cm × 1.5 cm platinum foil and 6 M KOH aqueous solution were served as reference, counter electrodes and electrolyte, respectively. The working electrodes were made by grinding mixing the samples, acetylene black as conductive material and poly(tetrafluoroethylene) (PTFE) as binder material with isopropanol in a mass ratio of 8:1:1 to form a homogeneous paste. After the added isopropanol was evaporated, the resulting paste was rolled into 10−20 $\mu$m thin film and then dried at 60 °C in vacuum for 12 h. The film was punched into 5 mm diameter wafer prior to being sandwiched into a pair of foamed Ni substrate (1 cm × 1 cm). The electrode was successfully prepared after pressing under a pressure of 10 MPa for 5 min.

Cyclic voltammetry (CV) was performed over a potential range of 0 to 0.60 V at a scan rate of 5.0 mV/s. Galvanostatic charge−discharge was tested in the sweep potential range of 0 to 0.50 V at various current densities. The specific capacitance, $C_{sc}$ (F/g), was calculated by the equations

$$C_{sc} = (I\Delta t)/(m\Delta V) \quad (1)$$

where $I$ is the constant current of discharging (A), $\Delta t$ is the time of discharging (s), $\Delta V$ is the difference of potential after a full discharge (V), and $m$ is the mass of the samples (g). Electrochemical impedance spectroscopy (EIS) was operated over the frequency range of $10^{-2}$−$10^5$ Hz with an ac voltage of 5.0 mV.

## 3. RESULTS AND DISCUSSION

**3.1. Characterization of Materials.** Figure 1 illustrates XRD patterns of the samples. The peaks appeared in the

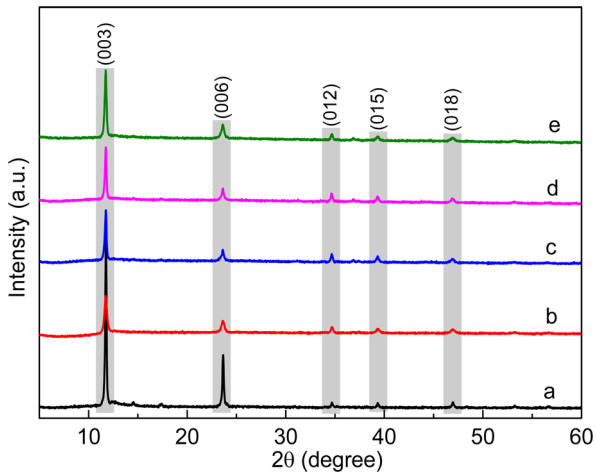


**Figure 1.** XRD patterns of pLH (a), LG (b), LFG-12 (c), LFG-18 (d), and LFG-24 (e).

pattern of pLH well agreed with the standard compound $Co_6Al_2CO_3(OH)_{16}{\cdot}H_2O$ (JCPDS card 51-0045) with the diffraction peaks appeared at $2\theta$ = 11.7° (003), 23.6° (006), 34.7° (012), 39.4° (015), and 47.0° (018), respectively, indicating that CoAl-LDH was generated.[14,18] Additionally, the interlayer spacing of (003) reflection plane was nearly 0.760 nm ascribed to the occupation of $CO_3^{2-}$ and $H_2O$ molecules in the interlamination.[11] In comparison, all peaks appeared in the spectra of the composites were in well agreement with those in


DOI: 10.1021/acsami.6b11316
ACS Appl. Mater. Interfaces 2017, 9, 5204−5212

pLH, indicating that CoAl-LDH generated during the second step of hydrothermal process. Furthermore, the intensity of (003) and (006) plane reflection peaks in the composites weakened after hybridizing with GN or FGN. These may be ascribed to that CoAl-LDH crystals deposited on GN or FGN sheets could prevent themselves from growing to be complete crystals, resulting in the much lower crystallinity.[17]

FT-IR spectra of the samples are shown in Figure 2. In Figure 2a, the spectrum of GN illustrated −OH stretching

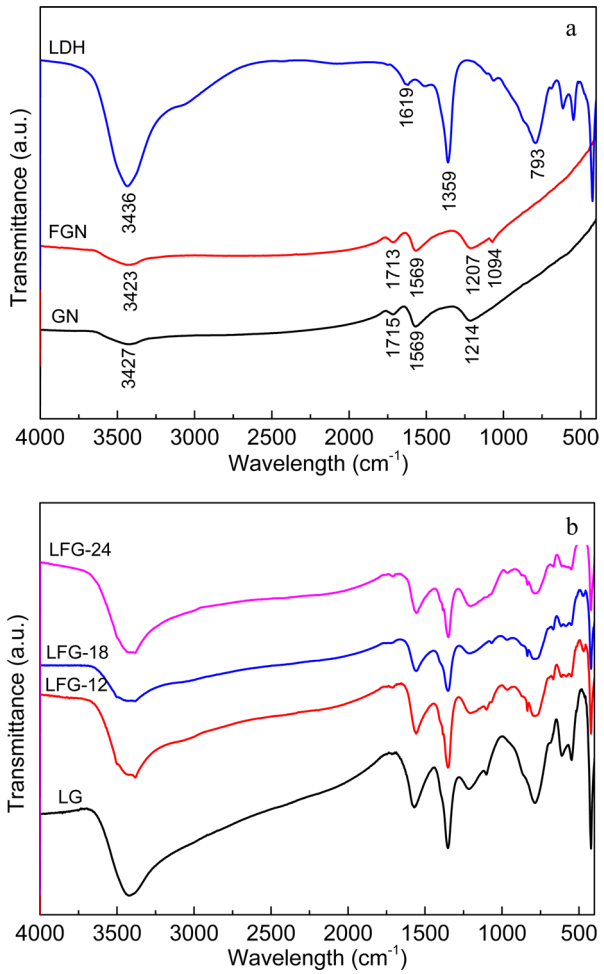


**Figure 2.** FT-IR spectra of pLH, GN, and FGN (a) and LG, LFG-12, LFG-18, and LFG-24 (b).

vibration at 3427 $cm^{-1}$, C═O (−COOH) stretching vibration at 1715 $cm^{-1}$, aromatic C═C stretching mode at 1569 $cm^{-1}$ ascribed from skeletal vibration of unoxidized graphitic domains, and C−O−C stretching vibration at 1214 $cm^{-1}$.[29] After fluorination, the peaks at 3423, 1713, 1569, 1207, and 1094 $cm^{-1}$ were observed in the spectrum of FGN, which were corresponding to −OH, C═O, aromatic C═C, covalent C−F, and semi-ionic C−F bonds, respectively.[24,30] The existence of C−F bonds with different configuration forms indicating that F atoms were grafted onto the framework of graphene during the process of fluorination. For pLH, the broad peak at 3436 $cm^{-1}$ belonged to O−H stretching vibration from H-bonded OH group and water molecules in the interlayer.[16] The peaks at 1359 and 793 $cm^{-1}$ could be assigned as the $\upsilon_3$ bending vibration of $CO_3^{2-}$.[2,31,32] All other peaks below 800 $cm^{-1}$ were ascribed to metal−oxygen (Me-O) stretching and bending vibration in the crystals.[2,32]

After hybridization, the characteristic peaks of pLH were still found in the spectra of the composites (as shown in Figure 2b), indicating that CoAl-LDH was successfully combined with GN or FGN. In addition, the peaks of aromatic C═C stretching mode at approximately 1560 $cm^{-1}$ were remained in the composites, and the peaks located at 1215 and 1089 $cm^{-1}$ originated from C−O−C and C−O were found in LG. In LFGs, the peaks at 1207 and 1102 $cm^{-1}$ nearby belonged to the covalent C−F and semi-ionic C−F bonds, respectively.[20,30] Moreover, the peak in the spectra of LFGs at 850 $cm^{-1}$ was attributed to the characteristic adsorption peak of carbonate anion.[31,32]

XPS analysis was used to accurately determine the composition and chemical bonds in LG and LFGs. As shown in Figure 3a, Co 2p and Al 2p peaks appeared in the survey spectra of the composites, suggesting the existence of CoAl-LDH in LG and LFGs composites. Furthermore, F 1s peaks were observed in the spectra of LFGs, proving that fluorination was successfully proceeding during the first step of hydrothermal process, corresponding well to the results of FT-IR analysis. In Figure 3b−e, the C 1s spectra of the composites were deconvoluted into several symmetrical peaks. In the case of LG, four peaks centered at 284.6 (C−C/C═C), 286.8 (C−O), 287.6 (C═O), and 289.6 eV (O−C═O) were observed.[33] After fluorination for various time, new peaks appeared at 289.1 eV (−CF) for LFG-12, 289.6 eV (−CF-$CF_2$), and 293.6 eV ($-CF_3$) for LFG-18, and 290.9 eV ($-CF_2$) and 292.2 eV ($-CF_3$) for LFG-24 were observed in Figure 3c−e.[34] It indicated that the −CF bonds were converted into $-CF_2$ or $-CF_3$ bonds as the fluorination time prolonged, which was in well agreement with previous reports.[34−36] The quantitative element composition of the composites obtained from the XPS analysis is shown in Table S1. The relative atomic amounts of C increased in the order of LG < LFG-12 < LFG-18 < LFG-24, while the relative atomic amounts of O decreased in the order of LG > LFG-12 > LFG-18 > LFG-24, indicating that the relative content of CoAl-LDH deposited on the surface of GN or FGN decreased in the order of LG > LFG-12 > LFG-18 > LFG-24. It may be due to that part of oxygenous functional groups on the GO surface were removed or bonded with F atoms in the first step of hydrothermal process, leading to the reduction of active sites for the adsorption of bivalent and trivalent cations.[34,37] The relative atomic amounts of F in LFG composites increased with the fluorination time, were 2.07% for LFG-12, 3.13% for LFG-18 and 4.22% for LFG-24, respectively.

The FESEM images of pLH and LFG-12, and TEM images of LFG-12 are shown in Figure 4. For pLH, most of the sheets were thin hexagonal shape with an average lateral size of nearly 1.5−4.0 $\mu$m, and agglomerated desultorily (Figure 4a), which was further illustrated by the TEM image of pLH as presented in Figure S1. The FESEM image of LFG-12 in Figure 4b showed that the thin sheets of CoAl-LDH were disorderly entangled with the corrugated and scrolled FGN sheets, and numerous pores existed in the composite. The measured specific surface area of LFG-12 was 76.30 $m^2/g$ (as shown in Figure S2). Compared to the sheets of pLH, the sheets of CoAl-LDH in LFG-12 composite were irregular, which may be attributed to the interaction between the CoAl-LDH and FGN sheets. The EDS spectrum in Figure S3 showed that the LFG-12 composite consisted of C, O, Co, Al, and F elements, indicating that CoAl-LDH and FGN coexisted in LFG-12,


DOI: 10.1021/acsami.6b11316
ACS Appl. Mater. Interfaces 2017, 9, 5204−5212

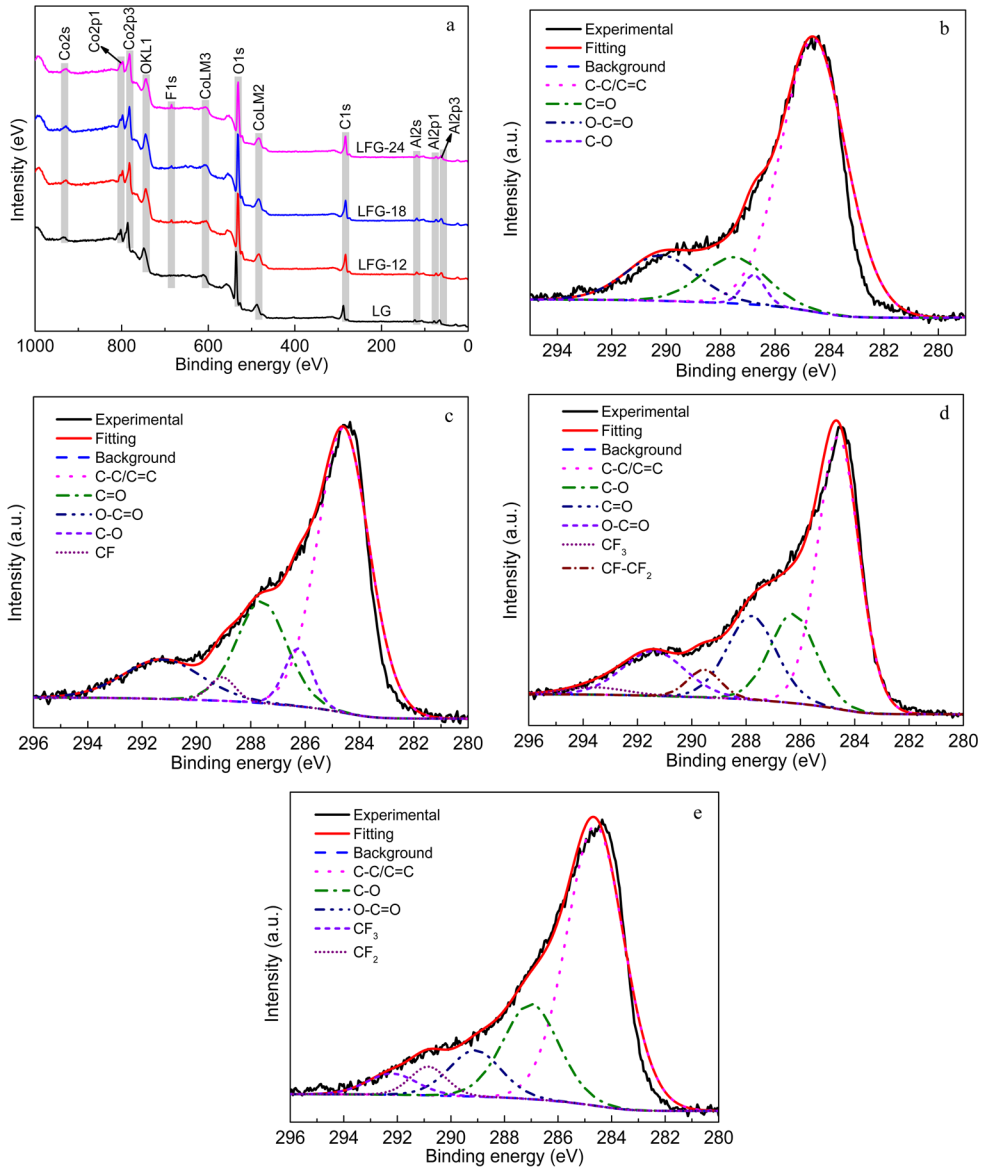


**Figure 3.** XPS survey spectra of the composites (a). C 1s XPS spectra of LG (b), LFG-12 (c), LFG-18 (d), and LFG-24 (e).

agreed well with the results of FT-IR and XPS analysis. The TEM image of LFG-12 in Figure 4c further shows that the sheets of CoAl-LDH were disorderly deposited on the wrinkled sheets of FGN which were approximately 2−3 layers (as shown in Figure 4d).

Based on the analysis mentioned above, the proposed synthesis process of LFG composite is shown in Scheme 1. During the first step of hydrothermal process, fluorine atoms were grafted onto the framework of graphene, and part of oxygenous functional groups on GO surface were removed simultaneously.[24,34] When $CoCl_2 \cdot 6H_2O$ and $AlCl_3 \cdot 6H_2O$ were mixed into the exfoliated FGN suspension, the positive $Co^{2+}$ and $Al^{3+}$ were first attached to the electronegative residual oxygenous functional groups ascribed to electrostatic attraction. Then, abundant nuclei formed and CoAl-LDH crystals grew on FGN surface through intermolecular H-bond or covalent coordination bond during the second step of hydrothermal process.[10] The in situ growth of CoAl-LDH crystals on FGN surface could not only hinder the agglomeration of FGN, but also obtain the desultorily dispersed CoAl-LDH crystallites with lamellar structure.[2]

**3.2. Electrochemical Measurements.** The CV curves of foamed Ni and pLH are shown in Figure S4. A weak pair of redox peaks was found in the curve of foamed Ni, which was caused by the presence of trace amounts of nickel oxide. In addition, pLH exhibited a notable redox process due to the reversible reactions of LDH-Co(II)/LDH($OH^-$)-Co(III) with $OH^-$.[10] Specifically, the current intensity of foamed Ni was far lower than that of pLH, indicating the capacitance originated from foamed Ni could be negligible compared to the total capacitance.

Figure 5a shows CV curves of pLH and the composites. An obvious pair of redox peaks were found in all the curves, indicating that Faradaic redox reactions were proceeding during the charge and discharge processes.[38] Based on the viewpoint proposed previously,[5,38,39] $OH^-$ ions could rapidly substitute the interlaminar anions once the electrode was immersed into the electrolyte (6 M KOH), so the redox reactions could be presented as


DOI: 10.1021/acsami.6b11316
ACS Appl. Mater. Interfaces 2017, 9, 5204−5212

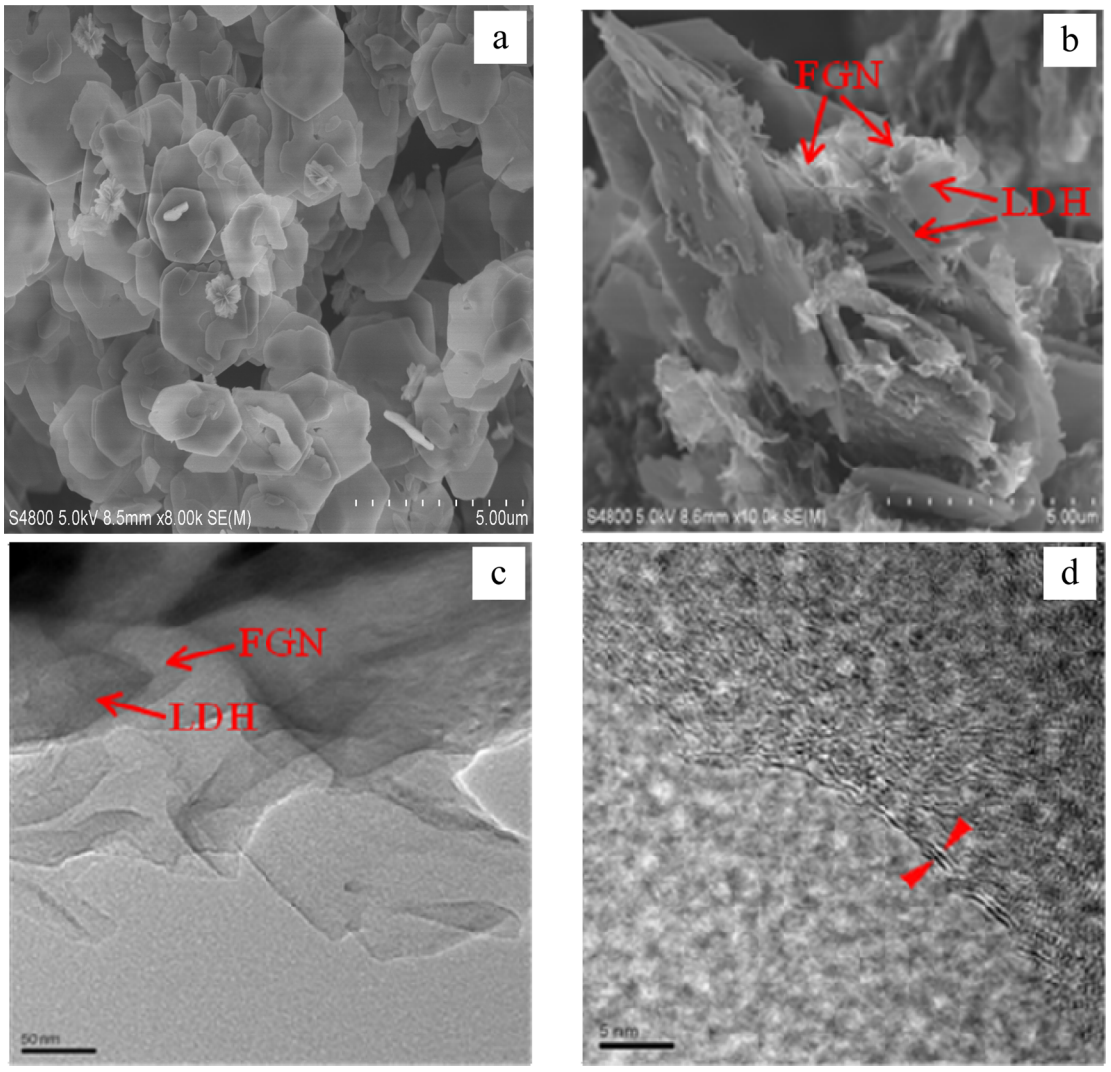


**Figure 4.** Typical FESEM images of pLH (a) and LFG-12 (b) and TEM images of LFG-12 (c and d).

**Scheme 1. Preparation Technique for the LFG Composites**

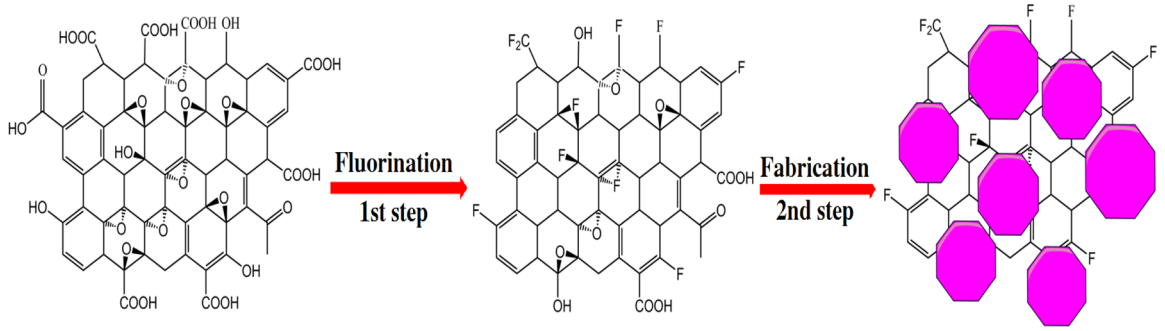


$$\text{LDH-Co(II)} + \text{OH}^-_{\text{sol}} \Leftrightarrow \text{LDH(OH}^-\text{)} - \text{Co(III)} + \text{e}^- \quad (2)$$

In addition, the redox potential positions of the composites were shifted a little which may be due to that the inherent phase stability of the CoAl-LDH in LG, LFG-12, LFG-18, and LFG-24 composites was worse and the crystallinity was lower when compared with pLH.[40,41] Furthermore, the integral areas of the CV curves increased in the order of pLH < LG < LFG-24 < LFG-18 < LFG-12, suggesting that the average capacitance of LFG-12 was the highest.

The galvanostatic charge−discharge curves of pLH and the composites are illustrated in Figure 5b. The charge−discharge curves were not ideal linear, which further confirmed that Faradaic reactions were proceeding during the processes.[10] The discharge time of LFG-12 was the longest, implying the best charge storage performance. At a current density of 1.0 A/g, the specific capacitances were calculated to be 620 F/g for pLH, 782 F/g for LG, 1222 F/g for LFG-12, 1028 F/g for LFG-18, and 894 F/g for LG-24 (as shown in Figure 5c). LG and LFGs composites exhibited higher specific capacitance when


DOI: 10.1021/acsami.6b11316
ACS Appl. Mater. Interfaces 2017, 9, 5204−5212

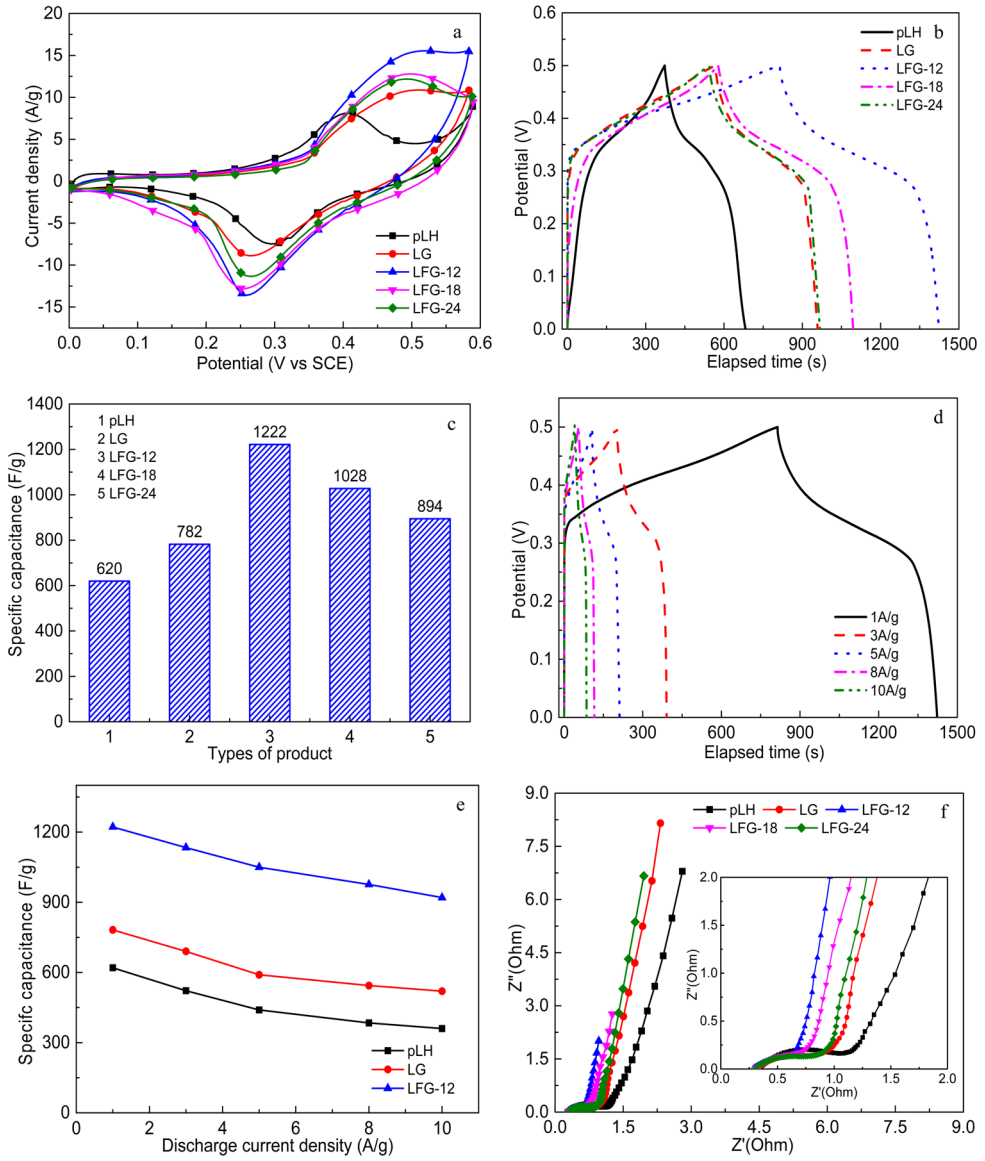


**Figure 5.** (a) CV curves of pLH and the composites at a scan rate of 5 mV/s. (b) Galvanostatic charge−discharge curves and (c) histogram of the specific capacitance of the samples at 1.0 A/g. (d) Galvanostatic charge−discharge curves of LFG-12 at various current densities. (e) Specific capacitances of pLH, LG, and LFG-12 at various current densities. (f) Nyquist plots of the EIS data for the samples.

compared with pLH, which was mainly ascribed to the synergetic effect between conductive GN or FGN and CoAl-LDH as reported previously.[10,11,28] Particularly, the GN or FGN in the composites has a superior electrical conductivity and can offer a conductive matrix for electron transportation during the electrode reaction processes.[10,28] Furthermore, it has been confirmed that the fluorine rich surface groups (such as $CF_2$, $CF_3$, etc.) hold insulating properties, leading to the decrease in electronic conductivity and transport property,[20,42,43] and the measured electrical conductivities of the composites were 113 S/m for LG, 197 S/m for LFG-12, 169 S/m for LFG-18, and 142 S/m for LFG-24. Thus, the differences in the specific capacitances of LFGs composites may be originated from the variety of fluorinated carbon configuration and fluorine content.

Figure 5d shows the galvanostatic charge−discharge curves of LFG-12 at various current densities, and the specific capacitances of LFG-12, LG, and pLH at various current densities are illustrated in Figure 5e. LFG-12 demonstrated evidently higher specific capacitances than that of pLH and LG at any current density. Furthermore, the specific capacitances of the samples decreased as the increasing current densities, which was ascribed to the resistance and insufficient Faradaic redox reactions under higher discharge current densities.[11] However, the decrease was significantly less for LFG-12 than those for LG and pLH with retention rates of 75.3%, 66.1%, and 57.9%, respectively. Thus, the rate capability of LFG-12 was remarkably enhanced compared with LG and pLH. It may be ascribed to that the excellent electrical conductivity and electrode stability of FGN, and the synergies of FGN and CoAl-LDH.[10]

Nyquist plots of the samples electrodes are presented in Figure 5f. The plots of all the samples contained an incomplete semicircle in the high-frequency range and a nonstraight line in the low-frequency region. The semicircle diameter represented the charge transfer resistance ($R_{ct}$) at the electrode/electrolyte interface originated from Faradaic reactions and double layer capacitance on the samples surface, while the slope of the line


DOI: 10.1021/acsami.6b11316
ACS Appl. Mater. Interfaces 2017, 9, 5204−5212

corresponded to capacitive behavior and ions diffusion resistance in the samples.[2,44] As shown in the inset part of Figure 5f, the diameters decreased in the order of pLH > LG > LFG-24 > LFG-18 > LFG-12 and the slope of LFG-12 was the greatest, indicating that LFG-12 hold the smallest $R_{ct}$, the best capacitive behavior, and the lowest ions diffusion resistance when compared with the other samples, leading to the highest reactivity and the fastest reaction kinetics. The results further indicated that LFG-12 possessed the enhanced ECPs suitable for the electrode material of supercapacitor.

To evaluate the cyclic stability, pLH, LG, and LFG-12 were tested for 3000 galvanostatic charge−discharge cycles at 10 A/g, and the results are illustrated in Figure 6. After 3000 cycles,

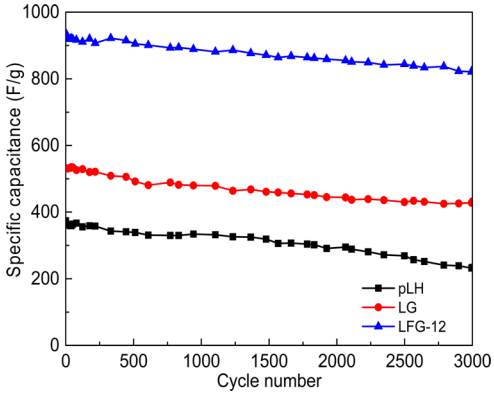


**Figure 6.** Cycle life of pLH, LG, and LFG at the current density of 10 A/g.

pLH, LG, and LFG-12 remained 62.6%, 81.2%, and 88.3% of their initial specific capacitance, respectively. LFG-12 composite exhibited clearly the best capacitance retention and the most ECPs stability than pLH and LG attributed to the high-efficiency electron and electrolyte transportation of FGN.[45]

Furthermore, XRD and FESEM were adopted to check the crystallographic structure and microstructure of the pLH and LFG-12 after a 3000 cycle test, to explore the reason for the decrease of capacitance retention. The FESEM images of pLH and LFG-12 after 3000 cycle tests at 10 A/g are shown in Figure 7. For pLH (Figure 7a), a large proportion of the sheets agglomerated more seriously and the average lateral size became smaller when compared with that in Figure 4a. As shown in Figure 7b, although the lateral size of CoAl-LDH sheets in LFG-12 was smaller and a few of agglomerates were formed, most of the porous structure was maintained after 3000 cycle tests.

Figure 8 shows the XRD patterns of the pLH (a) and LFG-12 (b) after a 3000 cycle test. As shown in Figure 8a and Table

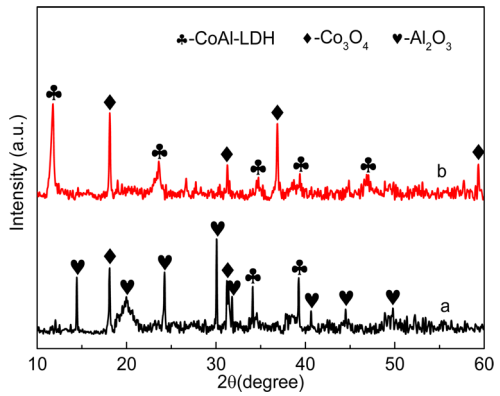


**Figure 8.** XRD patterns of the pLH (a) and LFG-12 (b) after a 3000 cycle test at 10 A/g.

S2, although the peaks corresponding to the (012) and (015) planes of CoAl-LDH (JCPDS card 51-0045) still presented in the pattern, most of the peaks corresponding to the reflection planes of $Co_3O_4$ (JCPDS card 43-1003) and $Al_2O_3$ (JCPDS card 88-0107) appeared when compared with that in Figure 1a. It indicated that most of the pLH crystals were destroyed and transformed into $Co_3O_4$ and $Al_2O_3$ in the charge and discharge processes. For the LFG-12 after 3000 cycle tests (Figure 8b and Table S2), most of the peaks corresponding to the reflection planes of CoAl-LDH were maintained, only few peaks assigned to the reflection planes of $Co_3O_4$ appeared, indicating that most of CoAl-LDH crystals remained the original crystallographic structure and a small number of them turned into $Co_3O_4$. Moreover, the variation of micromorphology and crystallo-

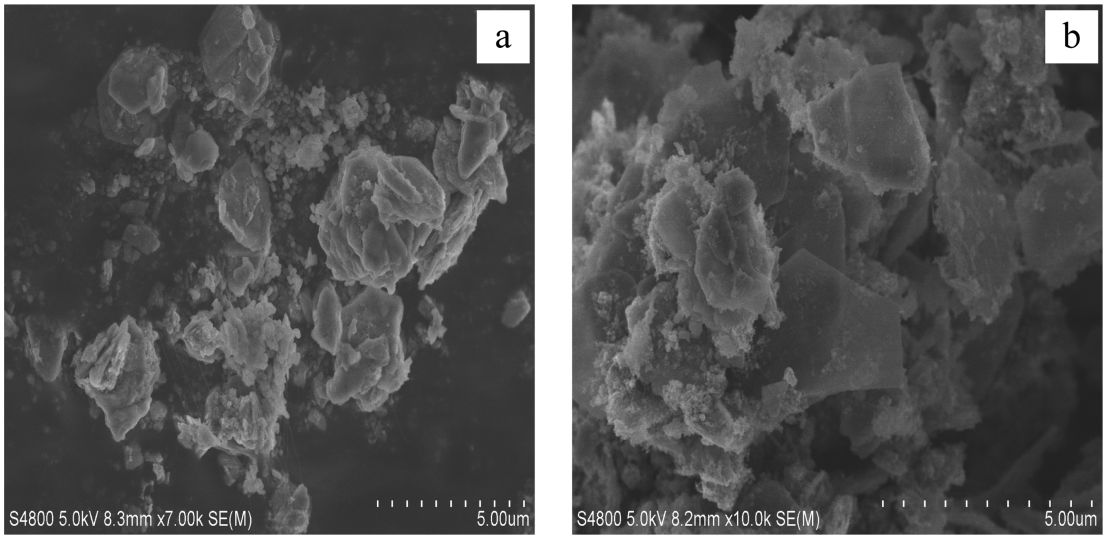


**Figure 7.** Typical FESEM images of pLH (a) and LFG-12 (b) after a 3000 cycle test at 10 A/g.



DOI: 10.1021/acsami.6b11316
ACS Appl. Mater. Interfaces 2017, 9, 5204−5212

graphic structure of the electroactive materials may be resulting in the reduction of capacitance retention in the cycle charge and discharge processes.

## 4. CONCLUSION

In this study, CoAl-LDH/FGN composites were successfully prepared using a two-step hydrothermal method. Fluorinated carbons with various configuration forms were generated on GN surface and part of the oxygenous functional groups was reduced during the first step of hydrothermal process. According to the analysis of XPS, LFG-12 possessed the most semi-ionic C−F bonds, and the fluorine rich surface groups (such as $CF_2$, $CF_3$, etc.) which were electrochemically inactive, were generated with the increase of fluorination time. During the second step of hydrothermal process, CoAl-LDH crystals were in situ anchored on the surface of exfoliated FGN. The superior electronic conductivity and transport performance of semi-ionic C−F bonds in LFG-12 composite endowed superior ECPs, like high specific capacitance, good rate capability and capacitance retention, making it become a potential electrode material for supercapacitors.

## ■ ASSOCIATED CONTENT

### Supporting Information

The Supporting Information is available free of charge on the ACS Publications website at DOI: 10.1021/acsami.6b11316.

Additional figures are TEM image of pLH, gas ($N_2$) adsorption isotherm loop for LFG-12, EDS scan area (a) and spectrum (b) of LFG-12, and CV curves of foamed Ni and pLH. In addition, tables of elemental composition of the prepared composites analyzed by XPS (at %) and phase analysis of the pLH and LFG-12 after 3000 cycle tests by XRD have been included (PDF)

## ■ AUTHOR INFORMATION


### Corresponding Author

*E-mail: ssx851215@whut.edu.cn.

### ORCID

Shaoxian Song: 0000-0001-7278-7875


### Notes

The authors declare no competing financial interest.

## ■ ACKNOWLEDGMENTS

The financial supports for the work from the National Natural Science Foundation of China under project nos. 51504176, 51474167, and 51674183 and Fundamental Research Funds for the Central Universities no. 2016-YB-026 are gratefully acknowledged. We also thank the Materials Research and Testing Center of Wuhan University of Technology.

## ■ REFERENCES


(1) Ramasahayam, S. K.; Nasini, U. B.; Shaikh, A. U.; Viswanathan, T. Novel Tannin-based Si, P Co-doped Carbon for Supercapacitor Applications. *J. Power Sources* **2015**, *275*, 835−844.

(2) Xu, J.; Gai, S.; He, F.; Niu, N.; Gao, P.; Chen, Y.; Yang, P. A Sandwich-type Three-dimensional Layered Double Hydroxide Nanosheet Array/Graphene Composite: Fabrication and High Supercapacitor Performance. *J. Mater. Chem. A* **2014**, *2* (4), 1022−1031.

(3) Simon, P.; Gogotsi, Y. Materials for Electrochemical Capacitors. *Nat. Mater.* **2008**, *7* (11), 845−854.

(4) Fan, Z.; Yan, J.; Wei, T.; Zhi, L.; Ning, G.; Li, T.; Wei, F. Asymmetric Supercapacitors Based on Graphene/MnO2 and Activated Carbon Nanofiber Electrodes with High Power and Energy Density. *Adv. Funct. Mater.* **2011**, *21* (12), 2366−2375.

(5) Su, L.-H.; Zhang, X.-G.; Liu, Y. Electrochemical Performance of Co−Al layered Double Hydroxide Nanosheets Mixed with Multiwall Carbon Nanotubes. *J. Solid State Electrochem.* **2008**, *12* (9), 1129−1134.

(6) Li, M.; Zhu, J. E.; Zhang, L.; Chen, X.; Zhang, H.; Zhang, F.; Xu, S.; Evans, D. G. Facile Synthesis of NiAl-layered Double Hydroxide/Graphene Hybrid with Enhanced Electrochemical Properties for Detection of Dopamine. *Nanoscale* **2011**, *3* (10), 4240−6.

(7) Zhang, F.; Zhao, L.; Chen, H.; Xu, S.; Evans, D. G.; Duan, X. Corrosion Resistance of Superhydrophobic Layered Double Hydroxide Films on Aluminum. *Angew. Chem., Int. Ed.* **2008**, *47* (13), 2466−2469.

(8) Gao, Z.; Wang, J.; Li, Z.; Yang, W.; Wang, B.; Hou, M.; He, Y.; Liu, Q.; Mann, T.; Yang, P.; Zhang, M.; Liu, L. Graphene Nanosheet/Ni2+/Al3+Layered Double-Hydroxide Composite as a Novel Electrode for a Supercapacitor. *Chem. Mater.* **2011**, *23* (15), 3509−3516.

(9) Liu, X.-M.; Zhang, Y.-H.; Zhang, X.-G.; Fu, S.-Y. Studies on Me/Al-layered Double Hydroxides (Me = Ni and Co) as Electrode Materials for Electrochemical Capacitors. *Electrochim. Acta* **2004**, *49* (19), 3137−3141.

(10) Zhang, L.; Zhang, X.; Shen, L.; Gao, B.; Hao, L.; Lu, X.; Zhang, F.; Ding, B.; Yuan, C. Enhanced High-current Capacitive Behavior of Graphene/CoAl-layered Double Hydroxide Composites as Electrode Material for Supercapacitors. *J. Power Sources* **2012**, *199*, 395−401.

(11) Fang, J.; Li, M.; Li, Q.; Zhang, W.; Shou, Q.; Liu, F.; Zhang, X.; Cheng, J. Microwave-assisted Synthesis of CoAl-layered Double Hydroxide/Graphene Oxide Composite and Its Application in Supercapacitors. *Electrochim. Acta* **2012**, *85*, 248−255.

(12) Malak-Polaczyk, A.; Vix-Guterl, C.; Frackowiak, E. Carbon/Layered Double Hydroxide (LDH) Composites for Supercapacitor Application†. *Energy Fuels* **2010**, *24* (6), 3346−3351.

(13) Yu, C.; Yang, J.; Zhao, C.; Fan, X.; Wang, G.; Qiu, J. Nanohybrids from NiCoAl-LDH Coupled with Carbon for Pseudocapacitors: Understanding the Role of Nano-structured Carbon. *Nanoscale* **2014**, *6* (6), 3097−104.

(14) Su, L.; Zhang, X.; Yuan, C.; Gao, B. Symmetric Self-hybrid Supercapacitor Consisting of Multiwall Carbon Nanotubes and Co−Al Layered Double Hydroxides. *J. Electrochem. Soc.* **2008**, *155* (2), A110−A114.

(15) Lai, F.; Huang, Y.; Miao, Y.-E.; Liu, T. Controllable Preparation of Multi-dimensional Hybrid Materials of Nickel-cobalt Layered Double Hydroxide Nanorods/Nanosheets on Electrospun Carbon Nanofibers for High-performance Supercapacitors. *Electrochim. Acta* **2015**, *174*, 456−463.

(16) He, F.; Hu, Z.; Liu, K.; Zhang, S.; Liu, H.; Sang, S. In Situ Fabrication of Nickel Aluminum-layered Double Hydroxide Nanosheets/Hollow Carbon Nanofibers Composite as a Novel Electrode Material for Supercapacitors. *J. Power Sources* **2014**, *267*, 188−196.

(17) Memon, J.; Sun, J.; Meng, D.; Ouyang, W.; Memon, M. A.; Huang, Y.; Yan, S.; Geng, J. Synthesis of Graphene/Ni−Al Layered Double Hydroxide Nanowires and Their Application as an Electrode Material for Supercapacitors. *J. Mater. Chem. A* **2014**, *2* (14), 5060.

(18) Kim, Y.; Kim, S. Direct Growth of Cobalt Aluminum Double Hydroxides on Graphene Nanosheets and the Capacitive Properties of the Resulting Composites. *Electrochim. Acta* **2015**, *163*, 252−259.

(19) Karlicky, F. s.; Kumara Ramanatha Datta, K.; Otyepka, M.; Zbŏril, R. Halogenated Graphenes: Rapidly Growing Family of Graphene Derivatives. *ACS Nano* **2013**, *7* (8), 6434−6464.

(20) Zhao, F.-G.; Zhao, G.; Liu, X.-H.; Ge, C.-W.; Wang, J.-T.; Li, B.-L.; Wang, Q.-G.; Li, W.-S.; Chen, Q.-Y. Fluorinated Graphene: Facile Solution Preparation and Tailorable Properties by Fluorine-content Tuning. *J. Mater. Chem. A* **2014**, *2* (23), 8782−8789.

(21) Jeon, I.-Y.; Ju, M. J.; Xu, J.; Choi, H.-J.; Seo, J.-M.; Kim, M.-J.; Choi, I. T.; Kim, H. M.; Kim, J. C.; Lee, J.-J.; Liu, H. K.; Kim, H. K.; Dou, S.; Dai, L.; Baek, J.-B. Edge-Fluorinated Graphene Nanoplatelets

as High Performance Electrodes for Dye-Sensitized Solar Cells and Lithium Ion Batteries. *Adv. Funct. Mater.* **2015**, *25* (8), 1170−1179.
(22) Li, Y.; Zhao, G.; Liu, C.; Wang, Y.; Sun, J.; Gu, Y.; Wang, Y.; Zeng, Z. The Structural and Electronic Properties of Li-doped Fluorinated Graphene and Its Application to Hydrogen Storage. *Int. J. Hydrogen Energy* **2012**, *37* (7), 5754−5761.
(23) Sun, X.; Song, P.; Zhang, Y.; Liu, C.; Xu, W.; Xing, W. A Class of High Performance Metal-free Oxygen Reduction Electrocatalysts Based on Cheap Carbon Blacks. *Sci. Rep.* **2013**, *3*, 2505.
(24) An, H.; Li, Y.; Long, P.; Gao, Y.; Qin, C.; Cao, C.; Feng, Y.; Feng, W. Hydrothermal Preparation of Fluorinated Graphene Hydrogel for High-performance Supercapacitors. *J. Power Sources* **2016**, *312*, 146−155.
(25) Peng, W.; Li, H.; Hu, Y.; Liu, Y.; Song, S. Characterisation of Reduced Graphene Oxides Prepared from Natural Flaky, Lump and Amorphous Graphites. *Mater. Res. Bull.* **2016**, *78*, 119−127.
(26) Peng, W.; Li, H.; Liu, Y.; Song, S. Comparison of Pb(II) Adsorption onto Graphene Oxide Prepared from Natural Graphites: Diagramming the Pb(II) Adsorption Sites. *Appl. Surf. Sci.* **2016**, *364*, 620−627.
(27) Hummers, W. S., Jr; Offeman, R. E. Preparation of Graphitic Oxide. *J. Am. Chem. Soc.* **1958**, *80* (6), 1339−1339.
(28) Zhang, L.; Wang, J.; Zhu, J.; Zhang, X.; San Hui, K.; Hui, K. N. 3D Porous Layered Double Hydroxides Grown on Graphene as Advanced Electrochemical Pseudocapacitor Materials. *J. Mater. Chem. A* **2013**, *1* (32), 9046.
(29) Chen, J.; Yao, B.; Li, C.; Shi, G. An Improved Hummers Method for Eco-friendly Synthesis of Graphene Oxide. *Carbon* **2013**, *64*, 225−229.
(30) Nakajima, T.; Gupta, V.; Ohzawa, Y.; Groult, H.; Mazej, Z.; Žemva, B. Influence of Cointercalated HF on the Electrochemical Behavior of Highly Fluorinated Graphite. *J. Power Sources* **2004**, *137* (1), 80−87.
(31) Cheng, J. P.; Liu, L.; Zhang, J.; Liu, F.; Zhang, X. B. Influences of Anion Exchange and Phase Transformation on the Supercapacitive Properties of α-Co(OH)2. *J. Electroanal. Chem.* **2014**, *722*−*723*, 23−31.
(32) Xie, R.; Fan, G.; Ma, Q.; Yang, L.; Li, F. Facile Synthesis and Enhanced Catalytic Performance of Graphene-supported Ni Nanocatalyst from a Layered Double Hydroxide-based Composite Precursor. *J. Mater. Chem. A* **2014**, *2* (21), 7880.
(33) Zhuo, Q.; Gao, J.; Peng, M.; Bai, L.; Deng, J.; Xia, Y.; Ma, Y.; Zhong, J.; Sun, X. Large-scale Synthesis of Graphene by the Reduction of Graphene Oxide at Room Temperature using Metal Nanoparticles as Catalyst. *Carbon* **2013**, *52*, 559−564.
(34) Wang, Z.; Wang, J.; Li, Z.; Gong, P.; Liu, X.; Zhang, L.; Ren, J.; Wang, H.; Yang, S. Synthesis of Fluorinated Graphene with Tunable Degree of Fluorination. *Carbon* **2012**, *50* (15), 5403−5410.
(35) Guérin, K.; Pinheiro, J.; Dubois, M.; Fawal, Z.; Masin, F.; Yazami, R.; Hamwi, A. Synthesis and Characterization of Highly Fluorinated Graphite Containing sp2 and sp3 Carbon. *Chem. Mater.* **2004**, *16* (9), 1786−1792.
(36) Wang, Y.; Lee, W. C.; Manga, K. K.; Ang, P. K.; Lu, J.; Liu, Y. P.; Lim, C. T.; Loh, K. P. Fluorinated Graphene for Promoting Neuro-induction of Stem Cells. *Adv. Mater.* **2012**, *24* (31), 4285−90.
(37) Vermisoglou, E. C.; Giannakopoulou, T.; Romanos, G.; Giannouri, M.; Boukos, N.; Lei, C.; Lekakou, C.; Trapalis, C. Effect of Hydrothermal Reaction Time and Alkaline Conditions on the Electrochemical Properties of Reduced Graphene Oxide. *Appl. Surf. Sci.* **2015**, *358*, 100−109.
(38) Huang, S.; Zhu, G. N.; Zhang, C.; Tjiu, W. W.; Xia, Y. Y.; Liu, T. Immobilization of Co-Al Layered Double Hydroxides on Graphene Oxide Nanosheets: Growth Mechanism and Supercapacitor Studies. *ACS Appl. Mater. Interfaces* **2012**, *4* (4), 2242−9.
(39) Scavetta, E.; Berrettoni, M.; Nobili, F.; Tonelli, D. Electrochemical Characterisation of Electrodes Modified with a Co/Al Hydrotalcite-like Compound. *Electrochim. Acta* **2005**, *50* (16−17), 3305−3311.
(40) Wimalasiri, Y.; Fan, R.; Zhao, X. S.; Zou, L. Assembly of Ni-Al Layered Double Hydroxide and Graphene Electrodes for Supercapacitors. *Electrochim. Acta* **2014**, *134*, 127−135.
(41) Wang, X.; Li, M.; Chang, Z.; Yang, Y.; Wu, Y.; Liu, X. Co3O4@MWCNT Nanocable as Cathode with Superior Electrochemical Performance for Supercapacitors. *ACS Appl. Mater. Interfaces* **2015**, *7* (4), 2280−5.
(42) Meduri, P.; Chen, H.; Xiao, J.; Martinez, J. J.; Carlson, T.; Zhang, J.-G.; Deng, Z. D. Tunable Electrochemical Properties of Fluorinated Graphene. *J. Mater. Chem. A* **2013**, *1* (27), 7866.
(43) Delabarre, C.; Dubois, M.; Giraudet, J.; Guérin, K.; Hamwi, A. Electrochemical Performance of Low Temperature Fluorinated Graphites Used as Cathode in Primary Lithium Batteries. *Carbon* **2006**, *44* (12), 2543−2548.
(44) Han, J.; Zhang, L. L.; Lee, S.; Oh, J.; Lee, K.-S.; Potts, J. R.; Ji, J.; Zhao, X.; Ruoff, R. S.; Park, S. Generation of B-doped Graphene Nanoplatelets Using a Solution Process and Their Supercapacitor Applications. *ACS Nano* **2013**, *7* (1), 19−26.
(45) Guérin, K.; Dubois, M.; Houdayer, A.; Hamwi, A. Applicative Performances of Fluorinated Carbons through Fluorination Routes: A Review. *J. Fluorine Chem.* **2012**, *134*, 11−17.


DOI: 10.1021/acsami.6b11316
*ACS Appl. Mater. Interfaces* 2017, 9, 5204−5212